Analysis of coherent radar sea clutter with combined wind driven sea and swell

Stephen Bocquet
Defence Science and Technology Group
Australia
ORCID 0000-0002-8026-8423

Luke Rosenberg
Defence Science and Technology Group
Australia
ORCID 0000-0002-2297-8355

Matthew Ritchie
Department of Electronic and Electrical Engineering
University College London
United Kingdom
ORCID 0000-0001-8423-8064

***Abstract*—Radar systems operating in a maritime environment need to be able to detect targets against a background of sea clutter returns. Hence it is important to understand the statistical behaviour of these returns in order to optimise a radar system detection algorithm. In this paper low and medium grazing angle radar sea clutter is analysed, to separate the effects of wind driven sea and swell in the Doppler spectrum. The offset gamma distribution is an effective model for the Doppler centroid and width distributions, as well as the asymmetric profile of the spectrum itself. The mean Doppler velocity is mostly due to the wind driven sea, with a contribution from the orbital velocity of the swell. A revised model is proposed for the mean Doppler shift as a function of grazing angle and azimuth.**

Keywords—radar, sea clutter, Doppler spectrum

I. INTRODUCTION

Maritime radar performance prediction requires accurate models of sea clutter. Limited data is available [1]; simulation allows a wider range of environmental conditions and geometries to be tested. Empirical models of sea clutter are much less technically demanding and computationally intensive than physical calculations of electromagnetic scattering from the sea surface, but the empirical parameters must be related to environmental conditions and geometry for the model to be useful. The sea surface will often be subject to both a wind driven sea and a swell. Empirical models for sea clutter tend to assume only a wind driven sea, or at least that the wind and wave directions are the same. In oceanic waters, or littoral waters exposed to ocean swell, the wind and wave directions are often different. The wind driven sea and swell affect the radar return in different ways, so it is desirable to have an empirical model for sea clutter that includes both explicitly.

A common modelling approach is to use the mean Doppler characteristics (width and centre point) to relate to the sea conditions. However, this does not capture the time- and range-varying fluctuations of the Doppler spectra, which are important for assessing the behaviour of coherent detection schemes. The evolving Doppler spectrum model [2],[3], offers a way to model these variations, with a moderate number of parameters. Recent models for the sea clutter Doppler spectrum are based on two components, representing 'slow' and 'fast' scatterers [2]. The slow component is mainly due to Bragg scattering from short gravity - capillary waves, while the fast component arises from breaking waves. From a practical point of view, two component models present difficulties due to the many parameters that must be related to environmental conditions and geometry. In the case of the evolving Doppler spectrum model, the complexity is reduced because the fast component only appears when the power in the slow component exceeds a threshold. The evolving Doppler spectrum model is one of the few models that actually link the model parameters to physical environmental conditions and geometry. However, the parameter model for the spatial correlation [3] is a simple negative exponential. This does not reproduce the cyclic patterns in the clutter due to the long wave. Further extensions are possible using more complex models for the texture, but these introduce additional parameters, and they are still not able to fully capture the detail required when determining the probability of detection for small targets.

In [4] a single component Doppler spectrum model was proposed. The Doppler spectrum was modelled with a single asymmetric component, with the parameters derived from memoryless non-linear transformations (MNLT) applied to a Gaussian random field representing the sea surface. The idea of an empirical model based on a simulation of the sea surface is appealing, because it could make use of the large body of oceanographic knowledge, resulting in fewer empirical parameters. This approach seems promising, but in [4] it was limited to the case where the wind, wave and radar look directions were aligned. The aim of this paper is to examine the general case, in order to understand how this simulation method could be extended.

Waves on three different length scales have particular effects on the radar return from the sea. Short gravity - capillary waves with half the transmitted wavelength of the radar give rise to Bragg scattering. These short waves are tilted and advected by both the long wave or swell, and by gravity waves of intermediate scale. Typically only the long waves are resolved by the radar. The short and intermediate scale waves are produced by the local wind at the sea surface. The radar return is modulated in both power and Doppler frequency by the long waves, which are not necessarily in the same direction as the local wind. It is the intermediate scale waves that break, producing whitecaps and stronger radar backscatter.

In this study two different data sets are examined, along with the published literature, to separate and quantify the effects of the wind driven sea and swell on the Doppler spectrum. The first data set was collected by the South African Council for Scientific and Industrial Research (CSIR) in 2007 using an X-band radar on Signal Hill, near Cape Town. The second data set was collected in 2004 and 2006 with the Australian Defence Science and Technology Group (DSTG) Ingara airborne X-band radar. The 2004 data were collected

from the Southern Ocean, near Port Lincoln, the 2006 data from the Timor Sea near Darwin.

II. CSIR Signal Hill Data

These data were collected with an experimental X-band radar deployed on Signal Hill, near Cape Town, in November 2007. Details of the radar, experimental set-up and environmental conditions during the trial are described in [5]. The data were previously studied in [6],[7] with reference to the sea clutter Doppler model proposed by Watts [8] and as part of a comparison of low and high grazing angle sea clutter. In this work, the same ten data files as [7] are analysed. The files are numbered 7-16, with the first five having a radar range of 58 km and the second five, 39 km. The files cover one quadrant in azimuth at 22.5° intervals, from 240° to 330°. Only vertical polarisation on transmit and receive is available, denoted VV.

A. *Doppler Spectra*

In previous work on another CSIR data set [4], it was discovered that the Doppler spectrum could be modelled with an offset gamma distribution, which has three parameters, shape, scale and offset, or equivalently, mean, standard deviation (SD) and offset. The empirical probability density functions (PDFs) of the Doppler centroid and width were also well described by offset gamma distributions. Fig. 1 shows the offset gamma distribution fits to the Doppler spectra and the centroid distributions for the Signal Hill data at 58 km range. The Doppler spectra are either left or right skewed, depending on the radar look direction with respect to the wind and waves. If the offset is positive, the spectrum is left skewed and the frequency scale must be reversed before fitting, because the gamma distribution is inherently right skewed. An example of the offset gamma distribution fit to the width PDF is shown in Fig. 2. Fig. 3 shows the means, SDs and gamma shape parameters obtained from the fits to the centroid and width distributions, for all ten files.

The mean Doppler in the wind direction is significantly greater at 58 km range than 39 km. This is likely to be due to the longer fetch at the longer range, leading to a more developed sea due to the wind [9]. The fetch is approximately the radar range, because the wind was directed offshore, with the radar location on Signal Hill within 2 km of the shore.

Poulter, Smith and McGregor [10] recorded asymmetric Doppler spectra from an S-band radar, from wind driven waves on an enclosed harbour. Their spectra have two well separated Bragg peaks, for waves travelling towards and away from the radar. Looking upwind, the peak corresponding to waves toward the radar is dominant, while in the downwind look direction the peak corresponding to waves travelling away from the radar is dominant. In the crosswind look direction both peaks are present, with about equal amplitude. The negative Doppler peaks are left skewed and the positive Doppler peaks right skewed. The usual convention is that motion toward the radar corresponds to positive Doppler and motion away from the radar, negative Doppler, but [10] adopt the opposite convention, with negative Doppler corresponding to motion towards the radar. When this is taken into account, the asymmetry and centre shifts of their Doppler spectra are consistent with the CSIR spectra. At X-band, the separation of the Bragg peaks is 0.46 ms^{-1}, or 31 Hz, so the two peaks are not resolved in the Doppler spectra. However, careful examination of the spectra suggests that they could be better represented as the sum of left and right skewed spectra, with

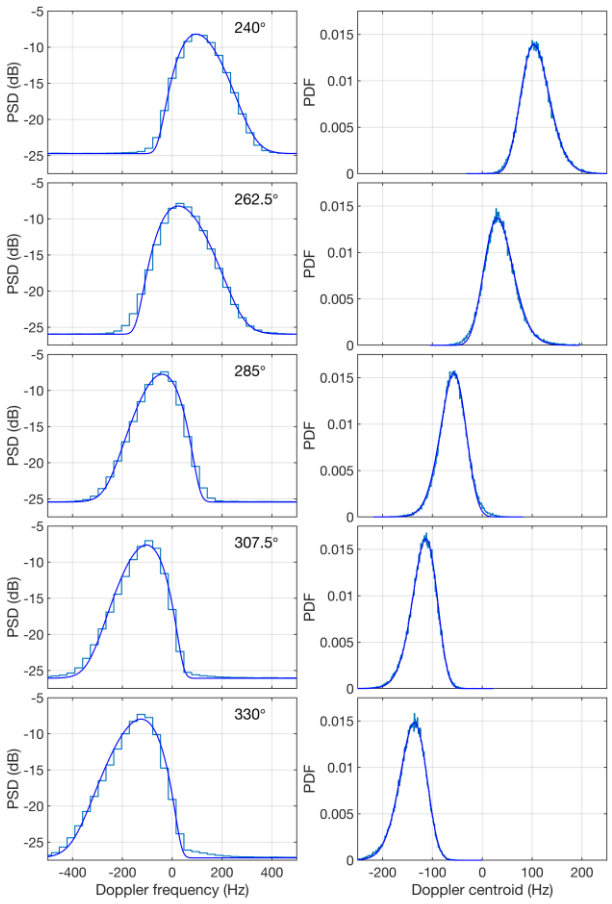

Fig. 1. Offset gamma distribution fits to Doppler spectrum (left) and centroid PDF (right), for files 7-11 (58 km range). Azimuth angles shown on spectrum plots at left. Data shown with staircase plots and fitted models with smooth curves.

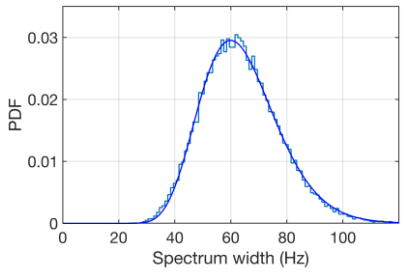

Fig. 2. Offset gamma distribution fit to Doppler width PDF for 240° azimuth and 58 km range.

the proportions varying with look direction. In the crosswind situation, the proportions are equal, so the overall spectrum is symmetric. Plant and Keller [11] recorded L-band Doppler spectra with separate Bragg peaks. They devised an empirical model for the azimuth variation in the amplitude of the two peaks to fit their data. Interestingly both peaks are present even in the upwind and downwind look directions, with the proportion of the smaller peak dropping to a few percent, but not zero. Poulter *et al.* [10] used an asymmetric Gaussian function to fit their spectra, i.e. a Gaussian with different widths on either side of the peak. The narrower of the two widths does not vary much with azimuth. The wider of the two varies in a manner consistent with broadening due to orbital velocities of short gravity waves that are not resolved by the radar. They attributed the different widths to shadowing, but this seems unlikely, because Plant and Farquharson [12] have

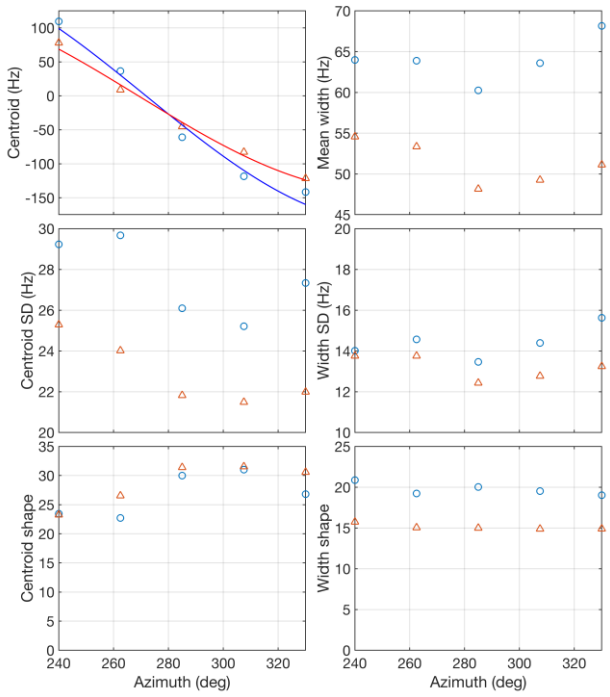

Fig. 3. Doppler centroid and width means, SD and shape parameters. Blue circles from 58 km range data, red triangles, 39 km range. Lines on centroid plot at top left are fits to sinusoidal variation in azimuth.

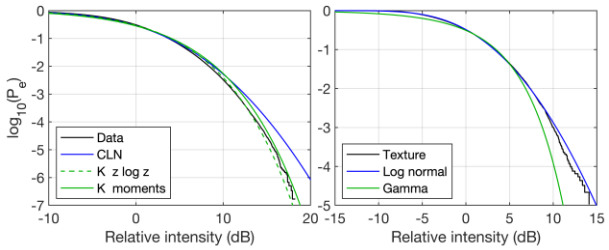

Fig. 4. CCDFs with estimated model distributions, for 240° azimuth and 58 km range. (Left) single pulse data, (right) texture.

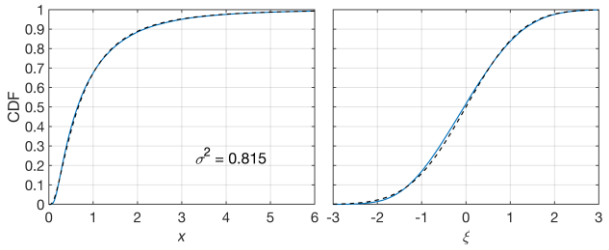

Fig. 5. Texture CDF, for 240° azimuth and 58 km range. (Left) Original data, dashed curve is log normal CDF for unit mean and $\sigma^2 = 0.815$. (Right) After application of MNLT to data, dashed curve is normal CDF for zero mean and unit variance.

since shown that shadowing is insignificant even at low grazing angles.

The mean width and centroid SD both dip at around 270° azimuth. Poulter *et al.* [10] found a similar dip in the spectrum width in the crosswind direction. Their data were collected in a harbour, with only a wind driven sea and no swell, so the wind and wave directions were the same. Here the wind direction is almost normal to the wave direction, so the "crosswind" azimuth is shifted towards the wave direction.

B. ω-k Plots

In [4],[13] a MNLT was applied to the clutter texture. The transformed texture is approximately normally distributed, and proportional to the sea surface slope over range and time, which facilitates calculation of the range - time autocorrelation function (ACF) and *ω-k* plot. The form of the MNLT depends on the empirical texture distribution. In [4] a gamma distribution gave the best fit, whereas in [13] a log normal distribution was used. Here the K distribution gives the best fit to the complementary cumulative distribution function (CCDF) from the single pulse intensity data (Fig. 4), with the shape parameter estimated from the first two intensity moments. The compound log normal (CLN) distribution overfits the tail. However, the log normal distribution gives a much better fit to the texture than the gamma distribution. Hence the log normal distribution is used for the MNLT applied to transform the texture variates x to normal variates ξ (Fig. 5), prior to calculating the ACF and *ω-k* plots.

The *ω-k* plots are shown in Fig. 6, for all ten data files. When the radar azimuth is close to the wave direction (235° azimuth), most of the power in the *ω-k* plot lies along the deep water dispersion curve. There is also a much weaker trace along the second harmonic of the dispersion curve, and significant power on a straight line through the origin. As the radar azimuth increases, the power along the dispersion curve disappears, leaving most of the intensity along the linear feature. The slope of this feature decreases and then becomes negative with increasing radar azimuth. This kind of linear feature in *ω-k* plots has been attributed to wave groups, with the slope being the group velocity. Fig. 7 shows the variation in the slope of this line with azimuth. However, the resulting group velocities are much less than the group velocity of the long wave. For example, the dominant wave in file 7 (240° azimuth, 58 km range) has a wavelength of 210 m and a group velocity of 9 ms^{-1}, but the slope of the 'group line' is 4.8 ms^{-1}. Plant and Farquharson [14] observed similar features in *ω-k* plots; they attributed the linear feature to short gravity waves, linked to wave breaking.

III. Ingara Data

These data were collected with the Ingara X-band airborne radar [15] in August 2004 and July 2006, off the coasts of Port Lincoln and Darwin, respectively. The data have been analysed in numerous studies since, see [2] for a summary of this work. The data used here were collected with all combinations of horizontal (H) and vertical (V) polarisation on transmit and receive.

The Ingara data were collected with the aircraft flying circular orbits around a patch of sea, so the collections cover 360° in azimuth. The circuits were flown at different altitudes and with different radii, yielding a range of grazing angles from 15° to 45°. There are two major difficulties in obtaining information on the sea clutter Doppler spectrum from the Ingara data. The aircraft speed was approximately 200 knots, so the Doppler shifts from the aircraft motion were much greater than those due to the motion of the sea surface, and it was not possible to get an absolute calibration of the sea clutter Doppler velocity. The pulse repetition frequency was variable, but approximately 300 Hz for the full polarisation data collections. The measured Doppler shifts often exceeded the available bandwidth, so the spectra are usually aliased. In previous work these difficulties were addressed by centring the spectrum to zero Doppler [16]. It was also discovered that

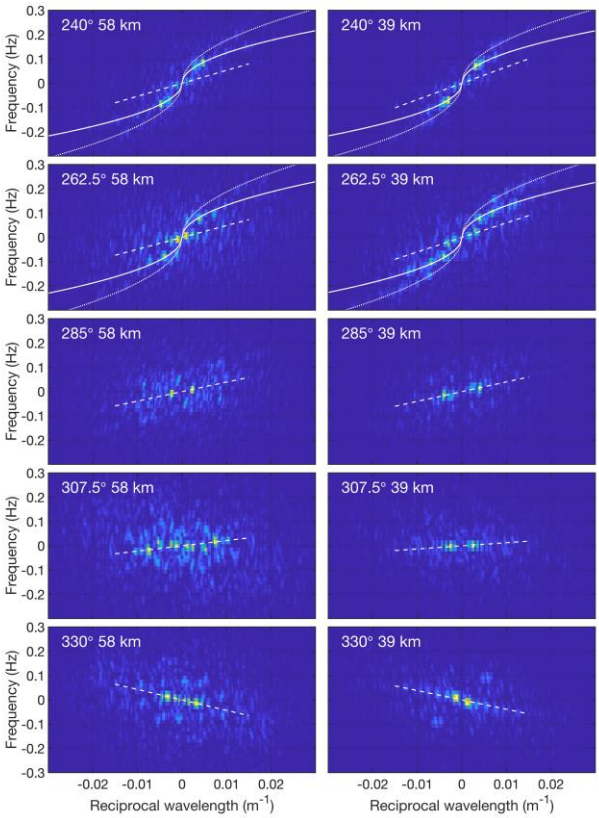

Fig. 6. ω-k plots. Solid curves in top four plots show the deep water dispersion relation; dotted curves show the second harmonic. The dashed lines are estimates of the 'group line'.

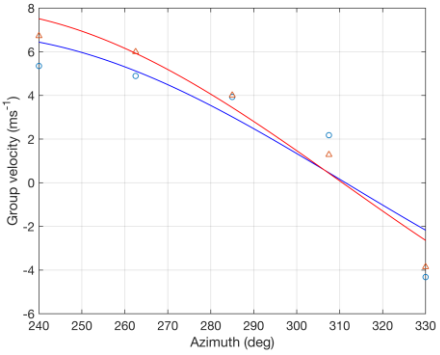

Fig. 7. Estimated group velocity (slope of the 'group line' in the ω-k plots). Blue circles from 58 km range data, red triangles, 39 km range. Curves are fitted sinusoids.

the cross pol Doppler shift did not always lie between the VV and HH channels, so it could not be relied on. Here the difference in mean Doppler between HH and VV is obtained, with the aliasing removed.

A. HH-VV Mean Doppler Difference

Fig. 8 shows the azimuth variation in the difference in mean Doppler between the HH and VV channels, for all runs in the F4 flight. This flight took place on 19 May 2006 over the Timor Sea. The azimuth φ is relative to the wind direction. Note that most runs contain more than one complete orbit. The variation in each run was fitted to a cosine function $a\cos(\varphi - \varphi_0) + b$, with amplitude a, offset b and phase φ_0. Fig. 9 shows a and b as a function of grazing angle θ for the F4 flight. The solid blue curve for the amplitude is a fit to the empirical model $a_0 \cos^4\theta$. The dashed blue curve shows the model from [17], $a_0 \cos 2\theta \cos\theta$, $\theta < 45°$. The model for the offset is described below. This fitting procedure was carried out for all runs in all 12 flights. Each flight took place on a different day, with a different wind speed over the sea. The estimated cosine amplitude at zero grazing, a_0, is proportional to the wind speed U, as shown in Fig. 10, with a constant of proportionality 0.11 ± 0.02.

There is a correlation between the offset b and the cosine amplitude a (Fig. 11). The offset becomes negative for low amplitudes, which correspond to low wind speeds and high grazing angles. Upwind - downwind asymmetry is a likely explanation for the offset. Smith *et al.* [18] measured the mean Doppler as a function of azimuth with a shore-based S-band radar, for a grazing angle of 6°. They found a significant upwind - downwind asymmetry with HH polarisation and a small asymmetry with VV polarisation. Here only the difference in mean Doppler between polarisations is obtained from the Ingara data. If the offset in HH polarisation drops off more rapidly with increasing grazing angle than the VV offset, the resulting offset in the HH-VV difference will become negative at higher grazing angles. Based on these ideas, the offset is modelled as $b = b_0 \cos\theta + b_1 a$, with the parameters b_0 and b_1 estimated by generalised linear regression. The red curve in Fig. 9 is calculated from this model, with $a = a_0 \cos^4\theta$. Across the 12 days of trial data, $b_0 = -0.33 \pm 0.09$ ms^{-1} and $b_1 = 0.66 \pm 0.20$. Although there is appreciable variation in both parameters, this does not appear to be related to wind speed or wave height. The value of b_0 indicates a much larger upwind - downwind asymmetry with VV polarisation than the 0.13 ms^{-1} measured in [18] for 10 ms^{-1} wind speed, so the offset model may not be correct.

B. Mean Doppler Azimuth

The phase φ_0 of the cosine fits is correlated with the relative wave direction (Fig. 12, left). This shows that the azimuth of greatest Doppler velocity is shifted slightly away from the wind direction, towards the wave direction. The phase is independent of grazing angle, so the values plotted in Fig. 12 are averages of all runs on each day.

The angle between the Doppler velocity vector and the wind direction can be estimated from the environmental parameters as follows. In most cases, the sea conditions can be represented as the superposition of a wind driven sea and a swell. If the wind driven sea is assumed to be fully developed, its significant wave height can be estimated as $H_w \sim 0.015\, U^2$, where U is the wind speed at 10 m above the sea surface [19]. The overall significant wave height is

$$H = \sqrt{H_w^2 + H_L^2}, \qquad (1)$$

where H_L is the significant wave height of the swell or long wave. Hence H_L can be estimated as

$$H_L = \sqrt{H^2 - H_w^2} \qquad (2)$$

provided $H > H_w$. The orbital velocity of the long wave is approximately $V_L = \pi H_L / T$, for wave period T. It has to be assumed that (i) the measured wave period is that of the long wave, and (ii) the wave direction is that of the long wave. The scatterer velocity in the wind direction has four contributions: (1) the Bragg velocity, 0.23 ms^{-1} at X-band; (2) the orbital velocity of the wind driven sea, ~0.1U, (3) wind drift ~0.03U, and (4) the 'fast scatterer' velocity, approximately the HH-

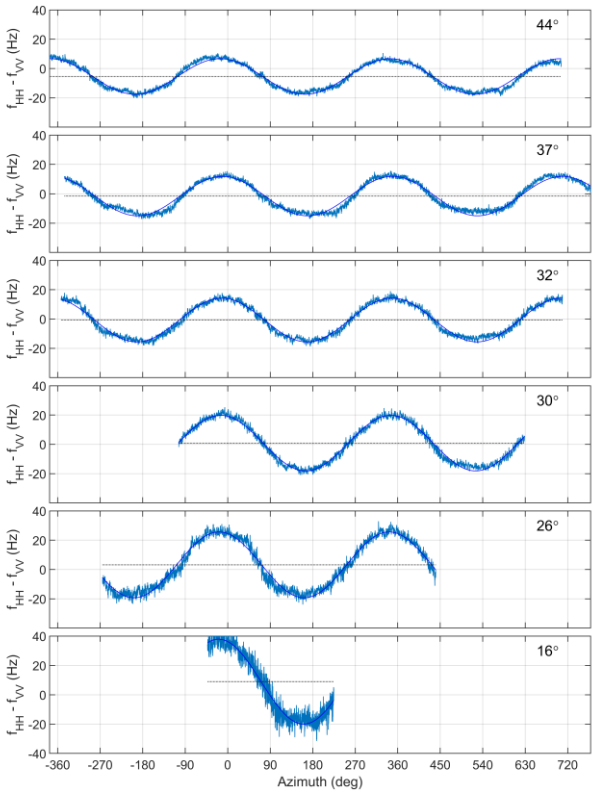

Fig. 8. Azimuth variation of HH – VV Doppler difference from F4 flight. Each plot shows a different run with a particular grazing angle.

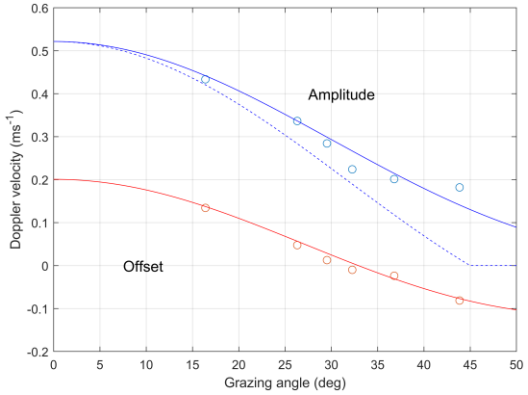

Fig. 9. Amplitude and offset from cosine fits to azimuth variation of HH – VV Doppler difference from F4 flight.

VV difference in Doppler velocity at zero grazing angle, a_0. Thus

$$V_w \approx 0.23 + 0.13U + a_0. \quad (3)$$

(Note that [2],[17] have $0.18U$ for the second term in (3), erroneously citing [19].) Then the sine and cosine rules can be applied to find the angle φ_2 between the resultant velocity vector and the wind direction. There are two days from the Darwin trial (flights F2 and F9) where the wind and wave directions were the same. In both cases $H_w > H$, so the above calculation does not work, and it can be inferred that there is only a wind driven sea, not fully developed, with no swell. Overall, the estimated angle φ_0 correlates fairly well with the calculated angle φ_2, as seen in Fig. 12 (right). Ideally $\varphi_0 = \varphi_2$, indicated by the line with unit slope. The RMS difference between φ_2 and φ_0 is 8°.

IV. Mean Doppler Model

The analysis of the Ingara data leads to the following revised model for the mean Doppler velocity. The total velocity in the plane of the sea surface is the vector sum $\mathbf{V_T} = \mathbf{V_w} + \mathbf{V_L}$, where $\mathbf{V_w}$ is the scatterer velocity due to the wind and $\mathbf{V_L}$ is that due to the orbital motion of the long wave. $\mathbf{V_L}$ has the same magnitude for both polarisations, $V_L = \pi H_L/T$. For VV polarisation, $V_w^{VV} = 0.23 + 0.13U$; for HH polarisation, $V_w^{HH} = 0.23 + (0.13 + 0.11\cos^3\theta)U$. The radial velocity parallel to the radar beam is $V_T \cos\theta \cos(\varphi - \varphi_0)$, where φ is the radar azimuth relative to the wind direction, and φ_0 is the azimuth of the total velocity relative to the wind direction.

V. Discussion and Conclusions

A simulation that correctly reproduces the spatial and temporal correlations due to the long waves or swell may require a time-varying simulation of a 2-D surface. This is somewhat cumbersome, because in general the sea surface is composed of both a wind driven sea and swell [20], with whitecaps resulting from interactions between the sea and swell [14]. Ideally the clutter simulation should be independent of the spatial and temporal resolution of the radar [21], but it may be possible to simplify the modelling with certain assumptions about the radar resolution. Real aperture radar typically has low resolution in azimuth, so the long waves are only resolved in range, and a time-varying range profile may be sufficient instead of a time-varying surface. Moreover, the wind driven sea may be not be resolved in range, depending on its state of development and the radar range resolution.

In the presence of both a wind driven sea and swell, the Doppler centroid of the clutter can be calculated as the vector sum of the wind-driven scatterer velocity and the orbital velocity of the swell. Analysis of the Ingara data leads to two modifications to the established empirical model for the mean Doppler. There is a small upwind - downwind asymmetry in the mean Doppler for VV polarisation, and a larger asymmetry for HH polarisation. The contribution to the HH mean Doppler from fast scatterers has approximately a $\cos^4\theta$ dependence on grazing angle θ. A separate model for the Doppler centroid is required for the evolving Doppler spectrum model, because it is based on analysis of the Ingara data with the Doppler spectrum centred to zero Doppler.

The width of the clutter Doppler spectrum does not vary greatly with azimuth, although it dips slightly when the radar look direction is perpendicular to the clutter velocity vector. The SD of the Doppler centroid has a similar azimuth variation. In general the clutter Doppler spectrum has an asymmetric profile, skewed in the direction of the total clutter velocity. An offset gamma distribution is an effective model for the Doppler centroid and width distributions, as well as the spectrum itself.

The full version of this paper will include an example of the offset gamma distribution fit to the Doppler spectrum from the Ingara data, to demonstrate that the asymmetry in the spectrum cannot be explained by shadowing, since it occurs at medium as well as low grazing angles.

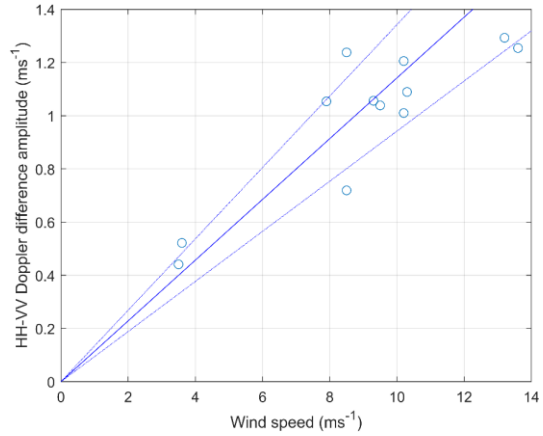

Fig. 10. Estimated HH – VV Doppler difference amplitude at zero grazing as a function of wind speed.

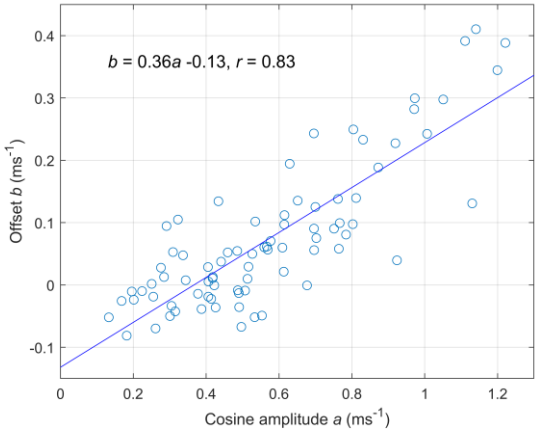

Fig. 11. Regression between offset and amplitude of cosine fits to azimuth variation of HH – VV Doppler difference.

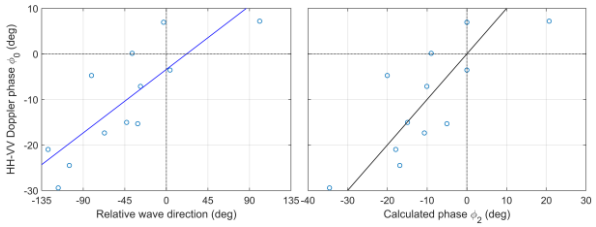

Fig. 12. Phase φ_0 of cosine fits to azimuth variation of HH – VV Doppler difference, plotted against (left) wave direction relative to wind azimuth, (right) calculated phase φ_2.

REFERENCES

[1] S. Watts and L. Rosenberg, "Challenges in radar sea clutter modelling," IET Radar Sonar Navig., vol. 16, no. 9, pp. 1403–1414, 2022.

[2] L. Rosenberg and S. Watts, Radar Sea Clutter: Modelling and Target Detection. London, U.K.: Inst. Eng. Technol., 2021.

[3] S. Watts, L. Rosenberg, S. Bocquet, and M. Ritchie, "The Doppler spectra of medium grazing angle sea clutter—Part 2: Model assessment," IET Radar Sonar Navig., vol. 10, no. 1, pp. 32–42, 2016.

[4] S. Bocquet, ″Analysis and simulation of low grazing angle X- band coherent radar sea clutter using memoryless nonlinear transformations,″ IEEE Trans. Geosci. Remote Sens., vol. 60, 2022, Art. no. 5111113, doi: 10.1109/TGRS.2022.3153632.

[5] P. L. Herselman, C. J. Baker and H. J. de Wind, "An Analysis of X-Band Calibrated Sea Clutter and Small Boat Reflectivity at Medium-to-Low Grazing Angles," International Journal of Navigation and Observation, pp. 1-14, 2008, doi:10.1155/2008/347518.

[6] M. A. Ritchie, A. G. Stove, S. Watts, K. Woodbridge, and H. D. Griffiths, "Application of a new sea clutter Doppler model," in IEEE International Radar Conference, 2013, pp. 560 – 565.

[7] M. A. Ritchie, H. D. Griffiths, S. Watts and L. Rosenberg, "Statistical comparison of low and high grazing angle sea clutter," Int. Conf. Radar 2014, October 2014.

[8] S. Watts, "Modeling and simulation of coherent sea clutter," IEEE Trans. Aerosp. Electron. Syst., vol. 48, no. 4, pp. 3303–3317, 2012.

[9] L. H. Holthuijsen, Waves in Oceanic and Coastal Waters. Cambridge, U.K.: Cambridge Univ. Press, 2007.

[10] E. M. Poulter, M. J. Smith and J. A. McGregor, "Microwave backscatter from the sea surface: Bragg scattering by short gravity waves," J. Geophys. Res., 99, C4, pp. 7929-7943, 1994.

[11] W. J. Plant and W. C. Keller, "Evidence of Bragg scattering in microwave Doppler spectra of sea return," J. Geophys. Res., 95, C9, pp. 16,299-16,310, 1990.

[12] W. J. Plant and G. Farquharson, "Wave shadowing and modulation of microwave backscatter from the ocean," J. Geophys. Res., 117, C08010, doi:10.1029/2012JC007912, 2012.

[13] S. Bocquet, ″Suzuki distributed monostatic and bistatic S-band radar sea clutter,″ IEEE Trans. Aerosp. Electron. Syst., vol. 59, no. 1, pp. 650–659, Feb. 2023.

[14] W. J. Plant and G. Farquharson, "Origins of features in wave number-frequency spectra of space-time images of the ocean," J. Geophys. Res., 117, C06015, doi:10.1029/2012JC007986, 2012.

[15] N. J. S. Stacy, D. P. Badger, A. S. Goh, M. Preiss and M. L. Williams, "The DSTO Ingara airborne X-band SAR polarimetric upgrade: first results," In Proceedings of the IEEE International Geoscience and Remote Sensing Symposium, Toulouse, France, 2003, pp. 4474–4476.

[16] L. Rosenberg, "Characterization of high grazing angle X-band sea-clutter Doppler spectra," IEEE Trans. Aerosp. Electron. Syst., 2014, 50, (1), pp. 406–417.

[17] K. Ward, R. Tough, and S. Watts, Sea Clutter: Scattering, The K-Distribution and Radar Performance, 2nd ed. London, U.K.: Inst. Eng. Technol., 2013.

[18] M. J. Smith, E. M. Poulter, and J. A. McGregor, "Doppler radar measurements of wave groups and breaking waves," J. Geophys. Res., 101, pp. 14269-14282, 1996.

[19] L. B. Wetzel, "Sea Clutter," in Radar Handbook, 2nd ed., M. I. Skolnik, Ed. McGraw-Hill, 1990, Ch. 13.

[20] S. Park and J. Park, "Realistic simulation of mixed sea using multiple spectrum-based wave systems," Simulation, vol. 96, no. 3, pp. 281–296, Mar. 2020.

[21] L. Rosenberg, "Parametric modeling of sea clutter Doppler spectra," IEEE Trans. Geosci. Remote Sens., vol. 60, pp. 1–9, 2022, doi: 10.1109/TGRS.2021.3107950.